

# Dynamic shear jamming under extension in dense granular suspensions

Sayantan Majumdar,<sup>1,\*</sup> Ivo R. Peters,<sup>1,2</sup> Endao Han,<sup>1</sup> and Heinrich M. Jaeger<sup>1</sup>

<sup>1</sup>*James Franck Institute, The University of Chicago, Chicago, Illinois 60637, USA.*

<sup>2</sup>*Engineering and the Environment, University of Southampton, Highfield, Southampton SO17 1BJ, UK*

Unlike dry granular materials, a dense granular suspension like cornstarch in water can strongly resist extensional flows. At low extension rates, such a suspension behaves like a viscous fluid, but rapid extension results in a response where stresses far exceed the predictions of lubrication hydrodynamics and capillarity. To understand this remarkable mechanical response, we experimentally measure the normal force imparted by a large bulk of the suspension on a plate moving vertically upward at a controlled velocity. We observe that above a velocity threshold, the peak force increases by orders of magnitude. Using fast ultrasound imaging we map out the local velocity profiles inside the suspension which reveal the formation of a growing jammed region under rapid extension. This region interacts with the rigid boundaries of the container through strong velocity gradients, suggesting a direct connection to the recently proposed shear-jamming mechanism.

PACS numbers: 82.70.Kj 83.60.Rs 83.50.Jf

Dense suspensions of hard particles in a simple liquid have the remarkably ability to transform from fluid to solid-like behavior when stressed. One well-known trigger for this solidification can be impact on the surface of such fluid [1], but perhaps even more intriguing is that solidification can also be observed under sufficiently fast extension [2–4]. Recent work has shown that impact-activated solidification (IAS) is a dynamic phenomenon connected to a rapidly propagating jamming front [1, 5, 6]. Here we consider the question whether similar jamming fronts also are responsible for solidification under extension.

As jamming fronts propagate into the bulk of a suspension, starting from the place at the suspension surface where strain was applied, they convert fluid material ahead of them into solid-like material in their wake. If such fronts are indeed created also under extension, then a situation would have to exist that at first glance appears quite counterintuitive: When the suspension surface is pulled upward, the front would need to move downward rather than propagating in the direction of the applied strain, as for IAS.

In this Letter we investigate the transient jamming dynamics of a large volume of suspension under extensional flow. We report the first observation of propagating jamming fronts under rapid extension. These fronts form the leading edge of a solid-like region that grows into the bulk of the suspension at a rate faster than the extension rate. Mapping out the flow field in the interior of the suspension with high-speed ultrasound imaging, we explicitly show that the fronts coincide with strong, localized shear. This suggests that the concept of shear jamming, originally developed for dry granular materials [7–9] but recently also identified as relevant for dense suspensions [5, 6] applies here as well.

When a front reaches the nearest rigid boundary of the container, the upward pulling force sharply increases, concomitant with a rapid slowing down of the entire ve-

locity field inside the suspension. The observed peak stress can reach  $\approx 70$  kPa (Fig. 1) transiently. Such value is much higher than reported previously for comparatively small cylindrical volumes under extension [2]. It is incompatible with explanations based on hydrodynamic lubrication between suspended particles [10] and also significantly exceeds capillary stresses due to menisci at the suspension surface [11]. Instead, such high values of peak stress can be explained by a model that treats the jammed region as a fully saturated porous medium and considers the stress required to displace interstitial liquid relative to the grains.

Our experiments use a prototypical suspension, cornstarch in water. Cornstarch particles have irregular shapes and range in size from  $5\mu\text{m}$  to  $20\mu\text{m}$  [12]. Suspensions are prepared by slowly adding cornstarch powder (Ingredion) for volume fractions ranging from  $\phi = 0.50 - 0.54$ , in a density matched ( $\rho = 1.6 \times 10^3 \text{ kg/m}^3$ ) solution of water, cesium chloride (CsCl) and glycerol. By varying the glycerol content, we can tune the solvent viscosity. Here, the solvent viscosity ranges from  $\eta = 10 \text{ mPas}$  to  $63 \text{ mPas}$ .

To study the force response under extension, we use a rheometer (MCR 301, Anton Paar). Unless otherwise specified, we use a circular plate of diameter 25 mm connected to the rheometer head through a rod (Fig. 1a). For a typical measurement, the plate is first placed on the surface of the suspension and the normal force ( $F_N$ ) is measured on the plate as it is pulled upward at constant velocity  $v$  (Fig. 1b) controlled through a feedback mechanism. The variation of  $F_N$  as a function of time is shown for two different pulling velocities in Fig. 1c for  $\phi = 0.52$ . We see a sharp rise in force for a pulling velocity of 8 mm/s, when the peak stress can reach  $\approx 70$  kPa. The peak stress is limited by the adhesion strength between the suspension and the plate [see Supplementary Information (S.I.)]. For  $v = 0.5 \text{ mm/s}$ , the peak force remains orders of magnitude lower. For granular suspen-

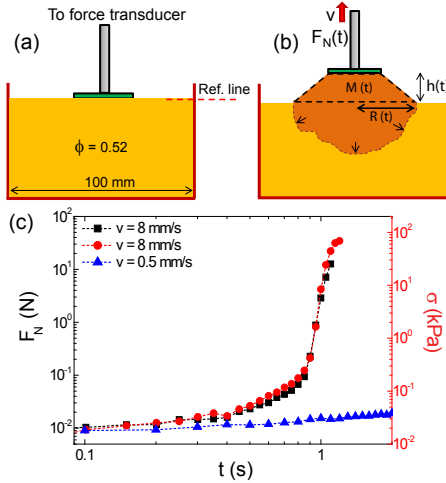


FIG. 1: (a) Schematic of the experimental set-up. (b) Formation of growing jamming front (brown colored region) under pulling. (c) Normal force and stress as a function of time for two pulling velocities. For  $v = 8$  mm/s, cases of weaker (black squares) and stronger (red circles) adhesion between plate and suspension are shown,  $\phi = 0.52$ ,  $\eta_s = 63$  mPa.s.

sions showing discontinuous shear thickening (DST), the maximum stress scale is provided by the confining capillary pressure at the suspension-air interface [10]. For our experiments, the observed peak stresses are much higher than the predicted capillary stresses ( $< 1$  kPa) [11]. Furthermore, covering the surface with solvent to suppress the capillary effects results in essentially the same extensional stress response, indicating that the static capillary stress is not controlling the maximum stress (S.I.). We first focus on the part of the suspension that is pulled out and above the bulk. To track the shape of this part, we use high speed video camera (Phantom V12, Vision Research). Typical images are shown in the inset of Fig. 2a. For lower pulling velocities ( $v < 3$  mm/s in this experiment; data not shown, but see S.I. Movie 2) the system behaves like a highly viscous liquid: under extension its contact line retracts towards the center of the plate and the suspension gradually flows back into the container. For  $v > 4$  mm/s, the contact line of the suspension with the plate remains pinned and only detaches after the rapid increase in force. This results in the formation of a jammed region whose shape we approximate by a truncated cone (Fig. 1b), which grows with time and maintains its shape under gravity (S.I. Movie1). Together with the high peak stress mentioned earlier, this is clear signature of a solid-like jammed state, because no fluid can maintain such shape under gravity.

Next, we calculate the instantaneous gravitational force on this jammed region having mass  $m(t)$  moving upward with a constant velocity  $v$ . The normal force on the plate is given by Newton's second law:

$$F_N(t) = d[m(t)v]/dt + m(t)g = vdm(t)/dt + m(t)g \quad (1)$$

Here, the mass  $m(t) = V(t)\rho$ , where  $V(t)$  is the volume of the jammed region pulled out of the bulk and  $\rho$  is the density of the suspension.  $V(t)$  can be estimated from geometry (Fig. 2):

$$V(t) \approx \frac{\pi[h(t) + \delta h(t)]}{3} [r(t)^2 + R(t)^2 + r(t)R(t)], \quad (2)$$

where  $r(t)$  and  $R(t)$  are the top and bottom radii of the frustum as determined from the tangent drawn at the middle of the curved surface of the frustum in the vertical plane (Fig. 2a),  $h(t)$  is the height of the plate measured from the rheometer data, and  $\delta h(t)$  gives the surface depression estimated geometrically from volume conservations (S.I.). To good approximation, the top radius is independent of time,  $r(t) \approx 0.8r_p$  ( $r_p$ : top plate radius). For the range of pulling velocities we use, the term  $m(t)g \gg v \cdot d[m(t)]/dt$ , thus,  $F_N(t) \sim m(t)g$ .

We compare the force calculated from the above model with the measured force in Fig. 2b. We find very good agreement at early times, demonstrating that the initial force evolution is dominated by the growing mass of the jammed region outside the bulk of the suspension. To explain the sharp rise in force under extension, we assume that, similar to the case of impact, the jamming front grows in all directions, including downward into the bulk (Fig. 1b), although the part that is growing inside the bulk cannot be seen optically because of the opaque nature of the suspension. As with IAS, the rapid rise in force then corresponds to the jamming front reaching the container bottom (or a side wall) [1, 5].

To test these assumptions, we map out the force response by varying the initial depth  $h_0$  of the suspension (Fig. 2c) for  $v = 8$  mm/s. The critical plate displacement ( $h_c$ ) at which force starts to rise sharply, increases as we increase  $h_0$ . Such delayed force rise with increasing suspension depth is consistent with a jamming front that propagates roughly at a constant velocity, similar to the case of impact [1, 5, 13]. Estimating the ratio of front to plate velocities,  $k = \frac{v_f}{v}$ , given by  $k = 1 + h_0/h_c$  for different  $h_0$  values, we find an average  $k = 6.5 \pm 0.7$  ( $\phi = 0.52$ ), indicating that the jamming front travels much faster than the pulling plate. This feature has also been observed under impact [1, 5, 13]. For a given  $h_0$ , the critical velocity ( $v_c$ ) for sharp rise in force decreases as a function of increasing volume fraction (Fig. 2d).

To understand the correlation between the observed force response and system dynamics, to visualize the jamming fronts, and to further explore connections to jamming under impact, we use fast ultrasound imaging (Verasonics Vantage 128, at up to 1,000 frames per second). This allows us to map out the flow profile by tracking the scattering from small air bubbles inside the suspension by using particle imaging velocimetry (PIV). In the ultrasound imaging set-up, the transducer is mounted underneath the suspension, facing upward to image a vertical slice in the same plane as the axis of the pulling plate.

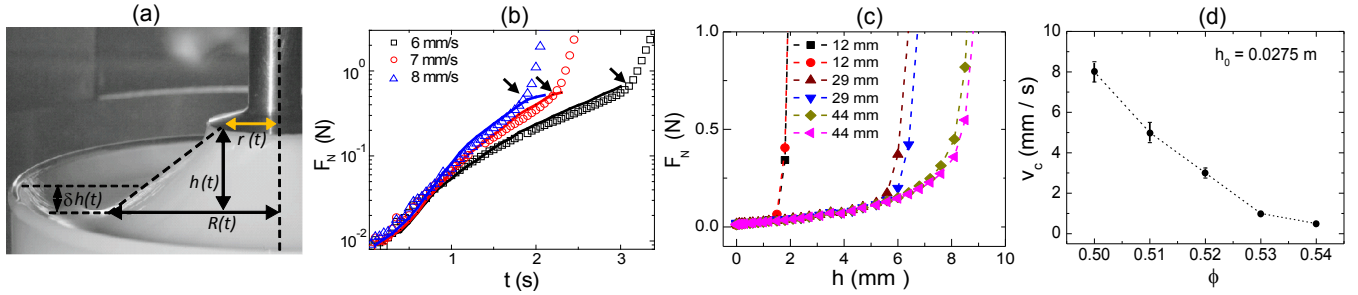


FIG. 2: (a) Geometrical parameters of the frustum shape formed by the suspension. (b) Force response as a function of time for different pulling velocities. Arrows indicate the onset of rapid increase in force. Solid lines indicate the model predictions. Here,  $\phi = 0.51$  and  $\eta_s = 50$  mPa.s. (c) Force response as a function of displacement for different initial depths ( $h_0$ ) of the suspension. For each depth, two consecutive measurements are shown. Here,  $\phi = 0.52$ . (d) Critical plate velocity ( $v_c$ ) for the onset of sharply increasing normal force for different volume fractions  $\phi$ ,  $h_0 = 27.5$  mm. The error bars correspond to the minimum velocity step size in going from a viscous like to a sharply increasing force response (each measured three times). The solvent viscosity  $\eta_s = 20$  mPa.s for both (c) and (d).

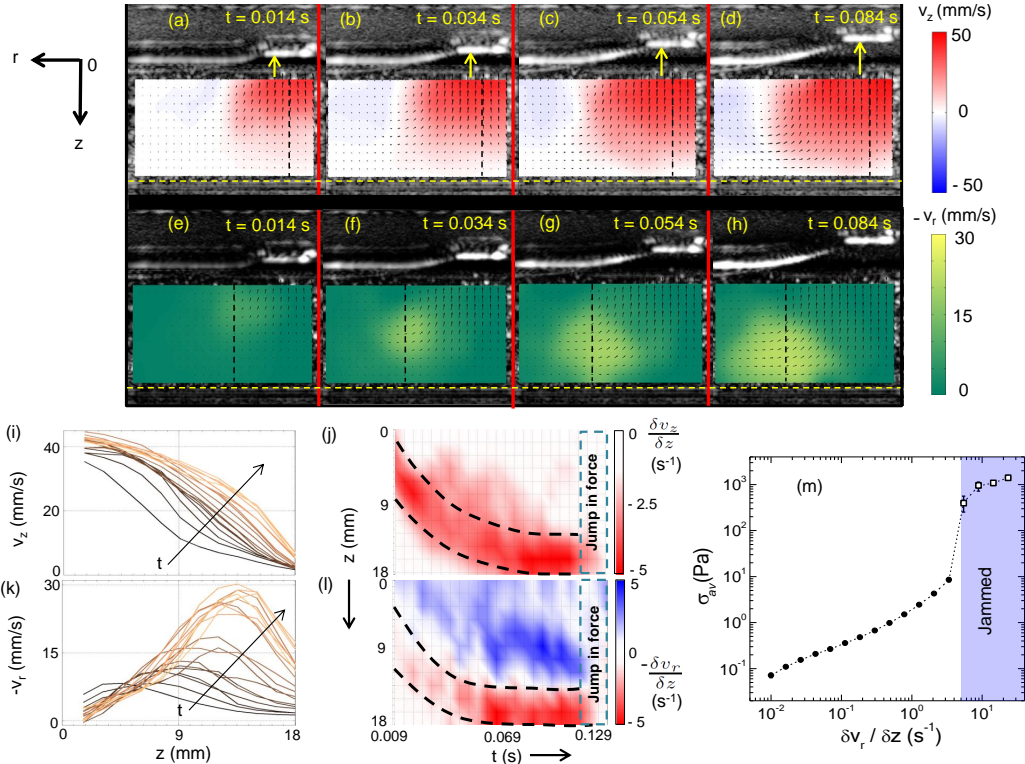


FIG. 3: (a) - (d) Time evolution of PIV vector field under extensional flow. Top plate starts to move at  $t = 0$  s with a velocity  $v = 50$  mm/s. Color indicates the vertical components ( $v_z$ ) of velocity. (e) - (h) Same vector field as before but color indicating the radial ( $-v_r$ ) velocity components. (i) Time evolution of  $v_z$  vs  $z$  and (j) space-time evolution of vertical velocity gradient  $\frac{\delta v_z}{\delta z}$ , along the dashed vertical lines in (a)-(d) for  $v = 50$  mm/s. Dark to light colors in (i) indicate increasing time from  $t = 0.009$  s to  $t = 0.104$  s in steps of 0.005 s. (k) Time evolution of  $-v_r$  vs  $z$  and (l) space-time evolution of radial velocity gradient  $-\frac{\delta v_r}{\delta z}$  along the dashed vertical lines in (e)-(h). (m) Shear-stress vs shear-rate measured under simple-shear. The shaded region indicates the shear-jammed state. Here,  $\phi = 0.50$  and  $\eta_s = 10$  mPa.s. Error bars indicate the standard deviations of three consecutive measurements.

Instead of using a rheometer, in these experiments a linear actuator (SCN5, Dyadic Systems) is used and the plate has 10 mm diameter. The PIV analysis window has size 36 mm  $\times$  20 mm (S.I.) with a spatial resolution of 1.5 mm  $\times$  1.5 mm. In Fig. 3a-d we show the velocity fields

at different instants of time inside a suspension with  $\phi = 0.50$  and  $\eta_s = 10$  mPa.s for a pulling velocity  $v = 50$  mm/s. The  $z$ -components of the velocity ( $v_z$ ) are color coded. We see a correlated region of high velocity that grows with time and finally interacts with the container

bottom (horizontal dashed lines in Fig. 3a-h) similar to the jammed region observed under impact [5]. In Fig. 3e-h, we show the same velocity profiles as in Fig. 3a-d but now with color indicating the radial velocity ( $-v_r$ ) component. We find that the maximum of  $|v_r|$  is localized near the edge of the jammed region and, as this region grows with time, the magnitude of  $v_r$  increases. We map out the time evolution of vertical ( $v_z$ ) and radial ( $-v_r$ ) velocity profiles as a function of depth ( $z$ ) in Fig. 3i and Fig. 3k, respectively, up to the point beyond which the entire velocity field within the PIV window suddenly slows down. At early times, when the front just starts to grow, the slope (gradient) of the velocity close to the bottom boundary of the container (larger values of  $z$ ) remains negligible compared to that near the plate (smaller values of  $z$ ), but at later times the gradient near the container boundary gradually becomes stronger. In contrast, for slow pulling velocities, where the normal force does not show any rise, the velocity gradient close to the rigid boundaries of the container remains negligible compared to that close to the moving plate at all times (S.I.).

The space-time evolution of the vertical velocity gradient  $\frac{dv_z}{dz}$  shows that a strong negative gradient localized at the front boundary (the region inside the black dashed-lines in Fig. 3j), which gradually approaches the bottom wall of the container. We can estimate the radial velocity gradient  $\frac{-\delta v_r}{\delta z}$  along the vertical line that contains the maximum of  $|v_r|$  (dashed vertical lines in Fig. 3e-h). The time evolution of  $\frac{-\delta v_r}{\delta z}$  (Fig. 3l), also shows a strong negative gradient approaching the bottom wall as a function of time.

The accumulation of a large shear rate at the front implies that the suspension can generate significant stresses, large enough to drive it into a solid-like jammed state. We can see this explicitly also in a separate experiment, where the same suspension is subjected to a steady-state shear ramp in a parallel plate rheometer (Fig. 3m). At shear rates of  $\sim 4 - 5 s^{-1}$ , corresponding to those at the front, the suspension behavior changes abruptly and the suspension enters a state where homogeneous flow is no longer possible and steady shearing initiates solid-like failure modes, such as partial detachment of the sample from the plate, slippage and formation of cracks (the maximum stress achievable with a transiently shear jammed state cannot be probed with steady state driving because of these failure modes; the measured values [open symbols in Fig. 3m] thus underestimate this stress].

The similarity between force response of dense suspension under impact [1, 5, 13] and extension sheds light on the jamming mechanism. In particular, it strongly supports the notion of jamming induced by shear [8, 9]. In our case, shear enters into the problem in a non-trivial way: localized strong shear at the boundary between the moving and the (still) unperturbed portion of the suspension gives rise to a growing jammed region through shear-induced network formation between par-

ticles [9, 14, 15]. The particles experience local stress levels sufficiently high to be pushed into frictional contacts, thereby breaching the lubrication barrier between them [16]. This stress is enabled by the inertia of the unperturbed suspension ahead of the front. Inside the bulk of the suspension, therefore, the flow field is essentially the same as under impact, but with the direction of flow reversed. When the jammed region reaches the container boundary, strong squeeze flow gives rise to strong shear that slows down the entire flow field due to shear jamming and gives rise to a solid-like contact network of particles extending from the bottom of the container to the top plate. Just before the detachment, the plate continues to move at a constant velocity and for maintaining continuity it tends to draw the solvent into the jammed network of particles. This is seen by a sudden change in surface texture of the frustum (from shiny to matte) just before the detachment (S.I.).

We estimate the average steady state pressure  $\Delta P$  (or stress  $\sigma$ ) at the top plate to suck the solvent (viscosity  $\eta_s$ ) through this jammed, porous medium, using a modified Kozeny - Carman relationship [17, 18]

$$\frac{\Delta P}{r_p} = \frac{60\eta_s\phi^2v_s}{\Xi^2a^2(1-\phi)^3}, \quad (3)$$

(see S.I.) where the sphericity parameter  $\Xi$  is of order unity,  $v_s$  is the solvent velocity, approximated by  $v$ , and  $a$  the particle diameter. We get a typical estimate for stress on the top plate  $\sigma \approx 3$  MPa (S.I.). However, this theoretical upper limit cannot be reached in practice because of other physical effects. In particular, the lower stress along the rim, due to the reduced path length, leads to breakage of the solvent layer at the rim before the maximum stress is reached. This can give rise to a dynamic delamination leading to eventual full detachment. While the exact mechanism remains to be explored, we believe that the competition between the dynamic delamination process and steady state solvent drainage sets the value of peak stress observed in our experiments. This is corroborated by the observation that the peak stresses scale linearly with  $v$  and  $\eta_s$  (see S.I.).

One very interesting question for future studies will be whether the dynamic jamming behavior observed here for non-Brownian suspensions will extend into the regime of dense colloidal systems, where the particles undergo Brownian motion. A recent computational study by Mari et al. [19] suggests that features such as the importance of frictional particle contacts should carry over. This would satisfy a key requirement for observing shear jamming over a sizable range in packing fractions [9]. Smith et al. [3] indeed observed jamming in colloidal systems under extension where brittle fracture happens at the neck region rather than at the top plate. However, how jamming fronts propagate and a dynamic shear jammed state is established and maintained in the presence of Brownian motion remains to be explored.

We thank Eric Brown, Nicole James, Shomeek Mukhopadhyay, Qin Xu, Tom Witten and Wendy Zhang for stimulating discussions. This work was supported by the Chicago MRSEC, which is funded by NSF through grant DMR-1420709. S.M. acknowledges support through a MRSEC Kadanoff-Rice fellowship.

---

\* majumdar@uchicago.edu

- [1] S. R. Waitukaitis and H. M. Jaeger, *Nature* **487**, 205 (2012).
- [2] E. E. B. White, M. Chellamuthu, and J. P. Rothstein, *Rheologica Acta* **49**, 119 (2010).
- [3] M. Smith, R. Besseling, M. Cates, and V. Bertola, *Nature Communications* **1**, 114 (2010).
- [4] M. Smith, *Scientific Reports* **5**, 14175 (2014).
- [5] I. R. Peters and H. M. Jaeger, *Soft Matter* **10**, 6564 (2014).
- [6] I. R. Peters, S. Majumdar, and H. M. Jaeger, *Nature*, DOI: 10.1038/nature17167 (to be published) (2016).
- [7] M. E. Cates, J. P. Wittmer, J.-P. Bouchaud, and P. Claudin, *Physical review letters* **81**, 1841 (1998).
- [8] N. Kumar and S. Luding, *arXiv preprint arXiv:1407.6167* (2015).
- [9] D. Bi, J. Zhang, B. Chakraborty, and R. Behringer, *Nature* **480**, 355 (2011).
- [10] E. Brown and H. M. Jaeger, *Reports on Progress in Physics* **77**, 046602 (2014).
- [11] E. Brown and H. M. Jaeger, *Journal of Rheology* **56**, 875 (2012).
- [12] A. Fall, N. Huang, F. Bertrand, G. Ovarlez, and D. Bonn, *Physical Review Letters* **100**, 018301 (2008).
- [13] S. R. Waitukaitis, *Impact-activated solidification of corn-starch and water suspensions* (Springer, 2014).
- [14] R. Seto, R. Mari, J. F. Morris, and M. M. Denn, *Physical review letters* **111**, 218301 (2013).
- [15] A. Fall, F. Bertrand, D. Hautemayou, C. Mezière, P. Moucheront, A. Lemaitre, and G. Ovarlez, *Physical Review Letters* **114**, 098301 (2015).
- [16] M. E. Cates and M. Wyart, *Rheologica Acta* **53**, 755 (2014).
- [17] W. L. McCabe, J. C. Smith, and P. Harriott, *Unit operations of chemical engineering* (McGraw-Hill, New York, 2005).
- [18] S. von Kann, J. H. Snoeijer, D. Lohse, and D. van der Meer, *Physical Review E* **84**, 060401 (2011).
- [19] R. Mari, R. Seto, J. F. Morris, and M. M. Denn, *Proceedings of the National Academy of Sciences* **112**, 15326 (2015).